Macromolecules

pubs.acs.org/Macromolecules Article

Origins of Charge Mobility Decreasing from Stretching−Releasing Cycles in Polymer Semiconductors

Xi Chen, Ke Li, Benzhi Min, Zibiao Li, Lian Duan, Haoyuan Li, and Shuzhou Li*

Cite This: https://doi.org/10.1021/acs.macromol.3c01071 Read Online

ACCESS | Metrics & More | Article Recommendations | Supporting Information

ABSTRACT: Polymer semiconductors as a key component of electronic skin need to maintain the coexistence of stretchability and electrical functionalities. However, repeated stretching−compressing cycles inevitably lead to the charge mobilities decreasing and poor working performance of polymer semiconductors. Here, a method combining molecular dynamics (MD) simulations and charge transport theory was developed to obtain the morphology−mobility relationship of amorphous poly(3-hexylthiophene) (P3HT). The simulation results show that the hole mobility decreases by 6% along the strain direction after three stretching−compressing cycles with 80% strain. These results are due to the chain alignment change caused by the mechanical operations. The stretched P3HT material presents higher charge mobility due to its better chain alignment, while the compressed P3HT shows lower charge mobility because of the poor chain alignment. Repeated stretching−compressing cycles lead to the chain alignment parameters decreasing along the deformation direction with accumulation and saturation effects. The repeated cycles also result in the primitive path length decreasing, which indicates polymer chain spatial distribution is more localized after repeated deformations. Our findings provide microscale knowledge about the dependence of molecular morphology and charge mobility on stretching−compressing cycles, which can help to guide the design of polymer semiconductors with higher charge mobility under repeated stretching−compressing cycles.

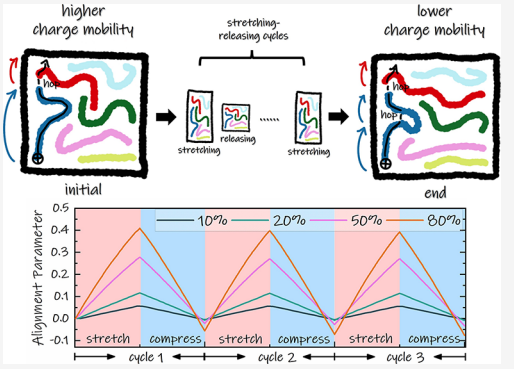

INTRODUCTION

Flexible electronics have great potential for next-generation wearable applications, such as electronic skin,[1] flexible display,[2] and flexible sensor.[3] It is essential that electronic materials can hold their electrical properties when they are frequently stretched during usage.[4] Among various materials, polymer semiconductors have emerged as a promising candidate due to their adjustable mechanical and electrical properties. However, the repeated stretching−compressing cycles inevitably lead to the electric functionalities degrading. It has been revealed that molecular structure design is an effective way to diminish this trend, such as backbone engineering, side-chain engineering,[5] and molecular weight optimization.[6] For example, introducing flexible nonconjugated spacers into the backbone can help to reduce elastic modulus and improve crack onset strain.[7−9] H-bonding[10] and metal−ligand coordination[11] can also act as crosslinking sites that provide reversible interactions between polymer chains. Although significant advances have been achieved in both the design and manufacturing of polymer semiconductors, there is still a big gap between the performance of lab-made materials and commercialization standards.

A better understanding of both charge-transport mechanisms and mechanical properties of polymer semiconductors from the microscale is needed for providing systematic guides to achieve further improvements. To this end, studies of polymer semiconductors focusing on either electrical properties or mechanical properties are intensely investigated through theory and simulations. It has been revealed that charge transport in polymer semiconductors shows multiscale characteristics. The overall charge mobility is determined by both the fast intrachain mobility and the much slower interchain charge hopping.[12] Therefore, the crystalline domains with ordered molecular arrangement provide effective ways for charge transport, while the amorphous regions are the main limit for achieving higher charge mobility. Tie chains, which effectively connect two crystal domains, provide effective charge transport in amorphous regions.[13] Besides, molecules with larger molecular weight are more likely to act as tie-chains which contribute to charge transport percolation[14] and higher charge mobility.[13,15] There are also a few theoretical studies focusing on the mechanical properties of polymer semiconductors.[16,17] It has been revealed that adding additives to poly(3-hexylthiophene) (P3HT) gives rise to the

Received: May 31, 2023
Revised: August 7, 2023

enhancement of tensile modulus due to the nonbonded interactions. Besides, the mechanical property also has a close relationship with the chain entanglement. The above research deepened our understanding of polymer semiconductors. However, the comprehensive knowledge of the dependence of electrical performance on morphology change caused by mechanical operations is still missing. The balance between electrical and mechanical functionalities is needed to design polymer semiconductors that can perform better when integrated into flexible electronics.

Here, we conducted a theoretical study combining molecular dynamics (MD) simulation and charge transport theory to investigate film morphology and charge mobility change after mechanical operations. Specifically, the morphology variation under strain was simulated through MD. Due to the high computational cost of all-atom (AA) MD simulations, we adopted the coarse grain (CG) model that has been proved to be able to predict the mechanical properties of P3HT.[16,17] In our MD simulations, we investigated two scenarios. In the first scenario, the equilibrium P3HT material was only stretched or compressed by a certain percentage to investigate the relationship between chain alignment and charge mobility. While in the second scenario, the equilibrium model was initially stretched by a certain percentage and then compressed to its original size. This process was carried out three times continuously, specifically, three stretching−compressing cycles. Here, instead of just releasing, the compression operation was applied to force the P3HT material to go back to its original size. The simulation results show that the charge mobility increases by 37% along the stretch direction when stretched by 80%, indicating a strong relationship between charge mobility and strain-induced morphology change. For P3HT material after three stretching−compressing cycles with 80% strain, the charge mobility decreased by 6%. With repeated stretching−compressing cycles, the chain alignment parameters decrease with accumulation and saturation effects. The primitive path lengths also decrease with repeated cycles. This means that the molecular chains' space distribution becomes localized. The above simulation results revealed the microscale mechanism of charge mobility decreasing with repeated stretching−compressing cycles.

METHODOLOGY

Molecular Dynamics. In this study, P3HT is chosen as the target system because it is one of the most widely studied polymer semiconductors with both experimental and theoretical methods. To get a better balance between computational cost and efficiency, various CG models have been developed to study different properties of P3HT.[18−25] Among these CG models, the three-site model is the most widely applied one to investigate not only self-assembly behavior[20,23] but also blends morphology[22,24] of P3HT. As illustrated in Figure 1a, in the three-site model, the P3HT monomer is represented with three beads: (1) the center of mass of the thiophene ring and the center of mass of carbon atoms of (2) the first three and (3) last three side-chain methyl groups.[18] This three-site CG model was originally developed with the Boltzmann inversion method and was able to reproduce the bond, angle, and dihedral distribution of the atomistic system.[18] This model was also verified to give equilibrium density and tensile modulus, which agree well with experimental results.[16,17] The parameters of this three-site CG model can be found in the Supporting Information and several previous studies.[15−18]

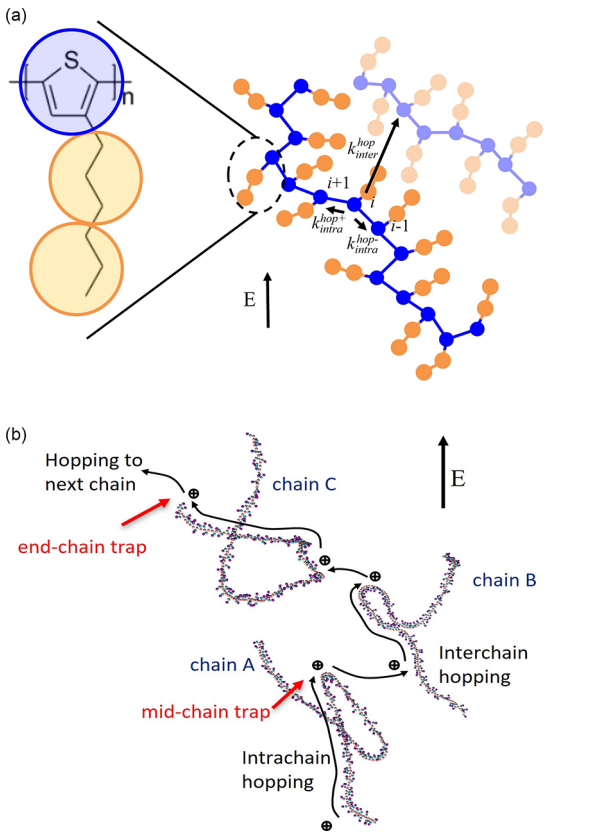

Figure 1. (a, b) Coarse grain model of P3HT and charge transport mechanism.

The modeling procedure is described as follows. Initially, 300 equilibrium P3HT molecular chains, each of which contains 150 monomers, were randomly packed into a periodic box with the Packmol package.[26] The initial density reached about 0.01 g/cm^3. Next, the whole system was relaxed at 600 K using the Langevin thermostat with the nonbonded interaction energy lowered to 10% of the condensed-phase value. This step lasted for 400 ns and enabled the system to explore the configuration space efficiently. Subsequently, the nonbonded interaction energy gradually increased to the condense-phase value using the Nose−Hoover style thermostat and barostat under 600 K and 1 atm, with the temperature and pressure damping parameters 400 and 4000 fs, respectively.[27] This densification process was performed with nine intervals with each interval 10% of the nonbonded interaction energy increased and each interval lasted for 20 ns. During each interval, the density was recorded to ensure that the system reached the equilibrium status under the corresponding condition. Finally, the system was then gradually cooled down to 300 K within another 60 ns. After that, a 40 ns simulation under 300 K was then conducted to further relax the system and generate the final equilibrium structure. The timestep of 4 fs and periodic boundary conditions were adopted during the whole process. The density finally stabilized at around 1.04 g/cm^3, which is very close to the value of 1.08 ± 0.02 g/cm^3 measured from the experiment.[28]

Finally, uniaxial deformations were applied to the quenched system along the z axis. Here, we investigated two scenarios. In the first scenario, the equilibrium geometry was only stretched or compressed to certain percentages to investigate the dependence of charge mobility on deformations. During

https://doi.org/10.1021/acs.macromol.3c01071
Macromolecules XXXX, XXX, XXX−XXX

deformation, a constant strain rate of 1×10^{-4} ps^{-1} was applied to the system along the z axis, while the pressure of 1 atm was always applied to the transverse direction. In this scenario, the simulated strain−stress curve is also recorded in Figure S1, which agrees well with previous simulation investigations.[16,17] In the second scenario, repeated stretching−compressing cycles were applied to the quenched system. It should be noted that the elastic range of bulk P3HT composing crystalline and amorphous regions is only about 2%.[29] Considering that polymer semiconductors are usually manufactured on an elastic substrate when the polymer semiconductors are stretched by a certain percentage, compressive deformation is then performed on the elongated material. Here, we adopt the same simulation steps for stretching and compressing the model. For example, if the system was stretched by 20%, then 2 ns were needed to fulfill both the stretching and compressing processes. This stretching−compressing operation cycle was performed three times continuously to evaluate the accumulation effect on molecule arrangement and charge transport. It is reported that the application range of flexible electronics is quite broad. In some cases, extremely high strain is anticipated such as strain sensor, while in other applications small strain but repetitive cycles are expected.[30] Specifically, flexible sensors with strain larger than 50% were needed to be successfully applied to full-range human activities' monitoring.[31] Therefore, different tensile strain rates, including 10, 20, 50, and 80% were considered in this study. The configurations during the deformation process were recorded for every 20,000 steps for further analysis. All the MD simulations and visualization were performed with LAMMPS[32,33] and VMD,[34] respectively.

Since this CG model of P3HT has never been applied to investigate structure change caused by stretching−compressing cycles, before the production run, we first made a validation of the CG model in describing the morphology change. This procedure was carried out by comparing the chain alignment parameter (see eq 6) variation with the results from the AA model. The chain alignment parameters within 3 stretching−compressing cycles with the strain of 50% of both the CG and AA model are illustrated in Figure S2. The chain alignment parameter change of the CG model agrees well with the results from the AA model. Therefore, further MD and charge transport simulations are all based on the CG configurations.

Charge Transport. The charge transport simulations were conducted based on Monte Carlo simulations combined with an off-lattice method which was initially proposed in ref 12. This off-lattice method has successfully revealed the multiscale charge transport characteristics of several organic semiconductors with different morphologies.[12,14,35,36] Here, we combined MD simulations and this off-lattice method to elucidate how mechanical operations affect charge transport mobility.

For one specific frame of configuration, the 300 P3HT molecules were extracted and each P3HT molecule was regarded as independent units. The CG model of P3HT and charge transport mechanism is illustrated in Figure 1. Each thiophene CG bead was regarded as a hopping site for the hole while the alkane side chains do not participate in charge transport. For one hole which is residing at position i, it has three hopping directions, position $i + 1$, $i - 1$ on the same chain, and another position on another chain, as shown in Figure 1a. The corresponding hopping rates are k_{intra}^{hop+}, k_{intra}^{hop-}, and k_{inter}^{hop}, respectively. It should be noted that the electronic orbital localization is highly sensitive to the intramolecular structure, especially the torsion angles.[37] The highest energy-occupied orbital of P3HT is usually within 5−7 monomers. This conclusion seems to contradict our assumption regarding each thiophene unit as a hopping site. However, this assumption does not change the charge-hopping nature of intrachain charge transport. Besides, considering that the intrachain charge transport mobility is 1−2 orders of magnitude larger than the interchain mobility,[38] this assumption will bring little error to the overall value of charge mobility.

As mentioned above, the charge transport in P3HT shows a significant multiscale characteristic.[38] This needs to be properly described by the charge transport model. It has been proved that the Marcus theory can describe this characteristic by using two sets of Marcus parameters.[12] Therefore, the charge transfer rates were calculated according to the Marcus theory.[39] Specifically, the charge transfer rate from site i to $i \pm 1$ was calculated according to eq 1, where J_{intra}^{hop} is the charge transfer integral between two adjacent thiophene structures, λ_{intra}^{hop} is the reorganization energy, k_B is the Boltzmann constant, and $\hbar$ is the reduced Planck's constant. The site energy difference $\Delta G_{intra}^{hop\pm}$ is given by $\Delta G_{intra}^{hop\pm} = Eq(z_{i\pm1} - z_i) = Eqd_i^{\pm}$ when electric field is applied along the z axis, while the inherent site energy difference between two hopping sites is not taken into account. Each thiophene unit also couples to a thiophene structure on another chain by considering the interchain charge transfer integral J_{inter}^{hop} and reorganization energy λ_{inter}^{hop}. The interchain site energy difference is calculated with a constant energy difference $\Delta G_{inter}^{hop} = Eq\gamma l_{bond}$, where γ is a ratio constant ($\gamma = 4.85$) and l_{bond} (= 3.865 Å) is the equilibrium distance between two neighbor thiophene CG beads taken from the MD force field. The electric field of $E = 0.06$ V/nm and temperature of $T = 300$ K were applied. It has been theoretically proved that large-scale hopping mobility depends on the average magnitude of inter-unit electronic coupling and is also independent of the electronic coupling distribution shape.[40] Therefore, only one group of Marcus parameters is utilized in this study, including the intrachain and interchain ones. These parameters include J_{intra}^{hop} (194 meV), λ_{intra}^{hop} (170 meV), J_{inter}^{hop} (2.4 meV), and λ_{inter}^{hop} (378 meV), which have been fitted for amorphous P3HT in the previous study[14] and are directly adopted in our simulations:

$$k_{intra}^{hop\pm} = \frac{(J_{intra}^{hop})^2}{\hbar}\sqrt{\frac{\pi}{\lambda_{intra}^{hop}k_BT}}\exp\left[-\frac{(\lambda_{intra}^{hop} + \Delta G_{intra}^{hop\pm})}{4k_BT\lambda_{intra}^{hop}}\right] \quad (1)$$

Another issue that should be confirmed is the transferability of these Marcus parameters to a stretched system since these parameters were fitted only for P3HT at the equilibrium state. In P3HT, both the inter-thiophene distance and dihedral angles will affect the charge transfer integral and charge mobility. The thiophene−thiophene distance and angle can be further divided into the interchain and intrachain parts. To validate the transferability of the Marcus parameters to stretched P3HT system, the structure comparison between the stretched and unstretched P3HT was conducted. The detailed information is elaborated in Section S5 of the Supporting Information. It was found that the inter-thiophene distance and dihedral angle distributions (for both intrachain and interchain) tend to keep unchanged during stretching.

https://doi.org/10.1021/acs.macromol.3c01071
Macromolecules XXXX, XXX, XXX−XXX

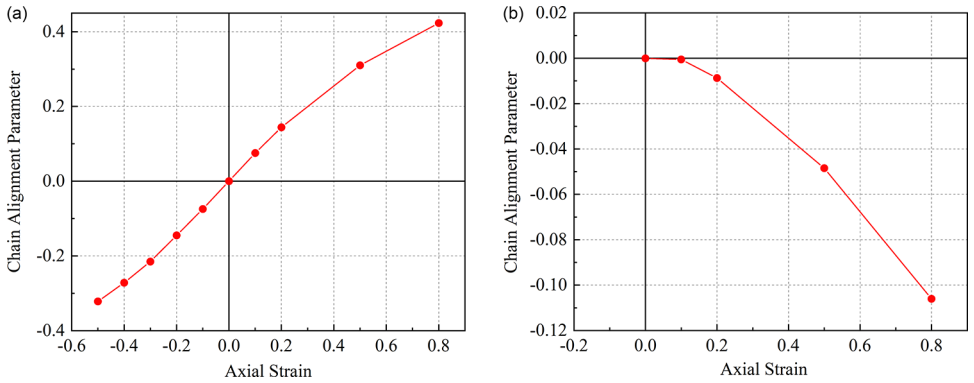

Figure 2. Chain alignment parameter of (a) scenario 1: only stretched or compressed P3HT material and (b) scenario 2: P3HT after three stretching−compressing cycles.

This means that the application of these Marcus parameters to a stretched P3HT system is reasonable.

The charge transport simulation was considered with the dynamic Monte Carlo method described as follows. The 300 P3HT chains in one configuration were first labeled from 1 to 300 and the thiophene CG beads on the same chain were also numbered from 1 to 150. At any point of charge transport simulation, only one P3HT molecule was under consideration. At the very beginning of simulations, the hole is placed on a random P3HT molecule with a random bead index. Then, the hole hops to the neighbor bead on the same chain under the motivation of the electric field and repeats this process until the hole hops to a new chain. Both the new chain number and bead index are then randomly determined. The interchain hopping distance, i.e., γl_{bond}, will be considered to calculate the moving distance and charge mobility. The hole is hopping among these 300 P3HT molecules and repeating the above process until certain criteria, e.g., distance or time, is met.

The charge transport process on MD-generated P3HT chains is shown in Figure 1b as an example. The hole is initially placed on a random position of chain A. Under the electric field, the hole will move along the chain until it meets a local "v" shape structure, which we call the mid-chain trap. The hole will reside at this place for a long time, waiting to hop to another chain. At one point, the hole is determined to hop to a random place on chain B and continue moving on. The hole can also move to the end of one molecule, i.e., end-chain trap, as denoted in Figure 1b. The trap density along the hole trajectory is the key factor that determines the overall charge mobility.

The hopping probability is randomly determined by the proportion of charge transfer rates, as illustrated by eq 2. The hopping time is calculated by eq 3. The hopping distance along the z axis and time of each step are recorded to calculate the charge mobility μ according to eq 4:[41]

$$P_k = \frac{k}{k_{intra}^{hop+} + k_{intra}^{hop-} + k_{inter}^{hop}}, \text{ where } k = k_{intra}^{hop+},\ k_{intra}^{hop-},\ \text{or } k_{inter}^{hop} \tag{2}$$

$$t_k = \frac{1}{k_{intra}^{hop+} + k_{intra}^{hop-} + k_{inter}^{hop}} \tag{3}$$

$$\mu = \lim_{t\to\infty} \mu(t) = \lim_{t\to\infty} \frac{z(t) - z(0)}{tE} \tag{4}$$

To get the time-dependent mobility, i.e., a statistically $\mu(t)$ relationship, the $z(t)$ is averaged from numerous trajectories, as shown in eq 5. For configurations before and after the stretching−compressing cycles with low strain, such as 10%, their configurational difference is tiny. Under this circumstance, the number of trajectories N is set rather large (about 7000) to distinguish the nuance of charge mobility. Besides, the random chain number and site index sequences were generated in advance. The hole was hopping according to the sequences for all configurations to minimize the random error when comparing different configurations:

$$z(t) = \lim_{N\to\infty} \frac{\sum_1^N z_i(t)}{N} \tag{5}$$

To present the change of chain alignment degree led by uniaxial deformations, we computed the chain alignment parameter P_{2x} according to eq 6. Here, the chain alignment parameter is computed and averaged over all thiophene units on all P3HT chains. The $\mathbf{e}_x$ represents the unit vector along the uniaxial deformation direction. The unit vector describing the local direction at each thiophene was computed from the chord connecting the two nearest neighbor thiophene CG beads: $\mathbf{e}_i = (\mathbf{r}_{i+1} - \mathbf{r}_{i-1})/|\mathbf{r}_{i+1} - \mathbf{r}_{i-1}|$. According to this equation, P_{2x} equals 1 when all the molecular chains are parallel with $\mathbf{e}_x$ and $-1/2$ when all the chains are perpendicular to $\mathbf{e}_x$. For fully random distributed molecular chains or amorphous phases, the corresponding P_{2x} equals 0:

$$P_{2x} = \frac{3}{2}\langle \mathbf{e}_i \cdot \mathbf{e}_x \rangle - \frac{1}{2} \tag{6}$$

RESULTS AND DISCUSSION

Figure 2 shows the chain alignment parameter of the first scenario and second scenario. As shown in Figure 2a, the chain alignment parameters show an increasing trend when the model is stretched and a decreasing trend when compressed. This result is consistent with the previous experimental study[16] and in accordance with expectations. This result also shows the huge impact of mechanical operations on molecular arrangement. When the model is stretched, the molecular chains present better alignment and wider spatial distribution along the stretching direction. Additionally, the saturation trend of P_{2x} gradually appears with the increase of axial strain since the chain alignment parameter is not linear with axial strain.

For the second scenario, the chain alignment parameter shows a different trend. As shown in Figure 2b, with increasing

https://doi.org/10.1021/acs.macromol.3c01071
Macromolecules XXXX, XXX, XXX−XXX

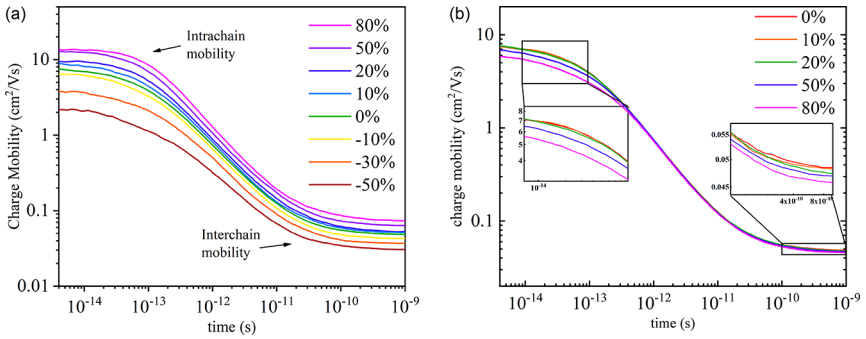

Figure 3. Time-dependent mobilities of P3HT from (a) first scenario and (b) second scenario.

deformation amplitude, the chain alignment parameter decreases rapidly. When the material is deformed with a small strain, such as 10%, the chain alignment parameter deviates little. However, after three times of repeating deformation cycles with 80% strain, the final chain alignment parameter reaches about −0.106. This result is even smaller than the value when the model is compressed by 10%, which is about −0.074. The parameter changes reveal how the stretching−compressing operations affect the space arrangement of molecular chains.

Figure 3 shows the time-dependent mobility of P3HT materials from both the first and second scenarios. For the stretched or compressed P3HT, as shown in Figure 3a, the strain percentages are labeled in the figure with the corresponding line color. Consistent with previous studies, the mobilities show two distinct regimes, the intrachain regime and the interchain regime. At short times or the intrachain regime, holes move along the backbone of P3HT without traps, exhibiting high mobility. At longer times or the interchain regime, the mobility decreases due to interchain hopping, which requires a longer time. Besides, the mobilities of stretched P3HT are overall larger than that of the original one, while the mobilities of compressed systems are overall smaller. This is qualitatively consistent with the previous experimental study about charge mobility anisotropy.[42]

For configurations after three times of stretching−compressing cycles, i.e., scenario 2, the multiscale mobilities are illustrated in Figure 3b. In both the intrachain regime and interchain regime, the mobility decreases along with the increasing deformation degree. Specifically, in the interchain regime, the mobility of the configurations with 10% strain is very close to the original, while the mobility with 20 and 50% deformation departures slightly. The configuration with 80% deformation shows the lowest mobility. Our simulation results are qualitatively consistent with the experimental phenomenon that the repeated stretch−release cycles will gradually lead to a decrease in charge mobility.[43] Considering the above discussions about chain alignment parameter change, it can be concluded that repeated deformations have a strong effect on the chain alignment parameter and therefore charge mobilities.

The chain alignment parameters discussed above only revealed the final effect brought by deformations. To elucidate the dynamic change of chain alignment parameters during stretching−compressing cycles, we calculated the parameters of each recorded structure, as shown in Figure 4. The stretching and compressing stages are colored pink and light blue and labeled with continuous cycles. The parameter variation shows two new characteristics, cumulative and

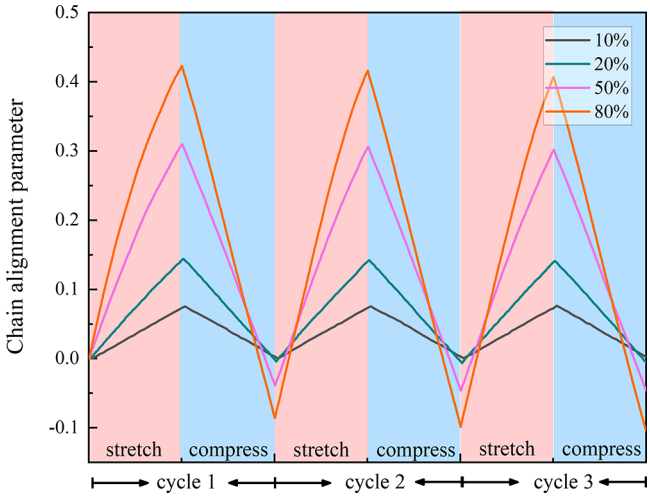

Figure 4. Dynamic change of chain alignment parameter with different strains.

saturation effects. For example, for the model with 80% strain, the chain alignment parameter changes from 0 to −0.086, −0.099, and finally −0.106 after each stretching−compressing cycle. After the first cycle, the parameter has a substantial change. Subsequent cycles further decrease the parameter with a smaller and smaller variation. Other lines with different strains also show the same trend.

It is speculated that the chain alignment parameter variations are highly correlated with permanent chain sliding. At the very beginning of stretching, the chains turned their alignment to the stretching direction, i.e., the z axis in our simulations. With the stretching deformation going on, the chain sliding inevitably occurred. However, since the P3HT chains are flexible instead of rigid, the chains cannot be inserted back into their original positions in the compressing process. Therefore, the chains tend to simply stack under the compressing force, resulting in the chain alignment parameter decreasing.

To further investigate the chain entanglement, we applied the Z1 code[44−47] to analyze the primitive path length (l_{pp}) change during the stretching−compressing cycles. The l_{pp} means the shortest path length that connects the two terminals of one chain without crossing over other chains. The l_{pp} was also calculated over all P3HT chains. Figure 5 shows the dynamic changes of l_{pp} during the deformation processes with 50 and 80% strain. Considering the complex interactions among the P3HT chains during deformation, l_{pp} also changes constantly within a range. The l_{pp} changes with 10 and 20% strain are not significant and thus are not displayed here. As

https://doi.org/10.1021/acs.macromol.3c01071
Macromolecules XXXX, XXX, XXX−XXX

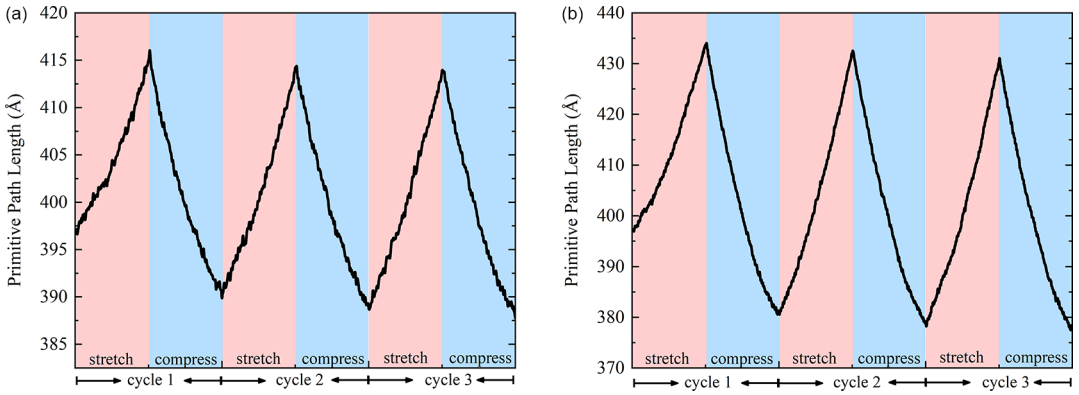

Figure 5. Dynamic change of the primitive path length during stretching−compressing cycles with (a) 50% and (b) 80% strain.

shown in Figure 5, l_{pp} increases during the stretching stage. This is because the stretching effect changes chains' alignment and reduces the entanglements among chains. It is within our expectations that the l_{pp} decreases in the compressing stage. However, the l_{pp} presents an overall downward trend over the repeated stretching−compressing cycles. This phenomenon demonstrates that the chains' spatial distribution becomes more localized. The P3HT material undergoing larger extent deformations shows a more significant change of l_{pp}, as illustrated in Figure 5b that the l_{pp} encountered a sharp drop from around 397 to 382 Å in the first stretching−compressing cycle.

CONCLUSIONS

In this study, we have developed a model combining charge transport theory and MD simulations to investigate the dependence of charge mobility on stretching−compressing cycles. It was revealed that charge mobility is highly correlated with chain alignment parameter change caused by mechanical operations. When P3HT material is only stretched or compressed, the charge mobility increases or decreases correspondingly along the stretching or compressing direction. The repeated stretching−compressing cycles also lead to the charge mobility decreasing. Specifically, our simulation results show that the hole mobility of P3HT decreases by 6% after three stretching−compressing cycles with 80% strain. The structural analysis shows that the repeated stretching−compressing cycles lead to the chain alignment parameter decreasing with accumulation and saturation effects. Besides, the primitive path length also decreases with repeated stretching−compressing cycles, indicating chain spatial distribution is more localized. Our simulation results provide microscale understandings of the dependence of molecular morphology and charge mobility on stretching−compressing cycles.

ASSOCIATED CONTENT

Supporting Information

The Supporting Information is available free of charge at https://pubs.acs.org/doi/10.1021/acs.macromol.3c01071.

Charge transport simulation code, equilibrium P3HT structure, and backmapping files (ZIP)

The coarse grain force field parameters of P3HT, simulated strain−stress curve, chain alignment parameters after each stretching−compressing cycle, backmapping method and AA simulation details, validation of Marcus parameters' application in the stretched system, and charge mobility anisotropy are provided (PDF)

AUTHOR INFORMATION

Corresponding Author

Shuzhou Li − *School of Materials Science and Engineering, Nanyang Technological University, Singapore 639798, Singapore;* orcid.org/0000-0002-2159-2602; Email: lisz@ntu.edu.sg

Authors

Xi Chen − *Institute of Flexible Electronics Technology of THU, Tsinghua University, Jiaxing, Zhejiang 314000, P.R. China; School of Materials Science and Engineering, Nanyang Technological University, Singapore 639798, Singapore*

Ke Li − *Institute of Materials Research and Engineering, Agency for Science, Technology and Research, Singapore 138634, Singapore;* orcid.org/0000-0002-3140-3983

Benzhi Min − *School of Materials Science and Engineering, Nanyang Technological University, Singapore 639798, Singapore*

Zibiao Li − *Institute of Materials Research and Engineering and Institute of Sustainability for Chemicals, Energy and Environment (ISCE2), Agency for Science, Technology and Research, Singapore 138634, Singapore;* orcid.org/0000-0002-0591-5328

Lian Duan − *Key Lab of Organic Optoelectronics and Molecular Engineering of Ministry of Education, Department of Chemistry, Tsinghua University, Beijing 100084, P. R. China; Laboratory of Flexible Electronics Technology, Tsinghua University, Beijing 100084, P.R. China;* orcid.org/0000-0002-7124-135X

Haoyuan Li − *School of Microelectronics, Shanghai University, Shanghai 201800, P.R. China;* orcid.org/0000-0002-2469-5842

Complete contact information is available at: https://pubs.acs.org/10.1021/acs.macromol.3c01071

Notes

The authors declare no competing financial interest.

ACKNOWLEDGMENTS

We thank the financial support from MOE Academic Research Fund Tier 2 (MOE-T2EP10220-0005). The computational resources are provided by the National Supercomputing

Centre Singapore (NSCC) and NTU High Performance Computing (HPC) cluster (Gekko). Chen Xi acknowledges the research scholarship awarded by the Institute of Flexible Electronics Technology of Tsinghua, Zhejiang (IFET-THU), Nanyang Technological University (NTU), and Qiantang Science and Technology Innovation Center, China (QSTIC). The authors thank Prof. David Huang for sending us the data files and parameters about the molecular dynamics. The authors also greatly appreciate Prof. Martin Kröger for providing us the executable Z1 code.

REFERENCES

(1) Chortos, A.; Liu, J.; Bao, Z. Pursuing prosthetic electronic skin. *Nat. Mater.* **2016**, *15*, 937−950.
(2) Zhang, Z.; Wang, W.; Jiang, Y.; Wang, Y. X.; Wu, Y.; Lai, J. C.; Niu, S.; Xu, C.; Shih, C. C.; Wang, C.; Yan, H.; Galuska, L.; Prine, N.; Wu, H. C.; Zhong, D.; Chen, G.; Matsuhisa, N.; Zheng, Y.; Yu, Z.; Wang, Y.; Dauskardt, R.; Gu, X.; Tok, J. B.; Bao, Z. High-brightness all-polymer stretchable LED with charge-trapping dilution. *Nature* **2022**, *603*, 624−630.
(3) Jiang, Y.; Zhang, Z.; Wang, Y. X.; Li, D.; Coen, C. T.; Hwaun, E.; Chen, G.; Wu, H. C.; Zhong, D.; Niu, S.; Wang, W.; Saberi, A.; Lai, J. C.; Wu, Y.; Wang, Y.; Trotsyuk, A. A.; Loh, K. Y.; Shih, C. C.; Xu, W.; Liang, K.; Zhang, K.; Bai, Y.; Gurusankar, G.; Hu, W.; Jia, W.; Cheng, Z.; Dauskardt, R. H.; Gurtner, G. C.; Tok, J. B.; Deisseroth, K.; Soltesz, I.; Bao, Z. Topological supramolecular network enabled high-conductivity, stretchable organic bioelectronics. *Science* **2022**, *375*, 1411−1417.
(4) Zheng, Y.; Zhang, S.; Tok, J. B.; Bao, Z. Molecular Design of Stretchable Polymer Semiconductors: Current Progress and Future Directions. *J. Am. Chem. Soc.* **2022**, *144*, 4699−4715.
(5) Mei, J.; Bao, Z. Side Chain Engineering in Solution-Processable Conjugated Polymers. *Chem. Mater.* **2014**, *26*, 604−615.
(6) Choi, J.; Kim, W.; Kim, D.; Kim, S.; Chae, J.; Choi, S. Q.; Kim, F. S.; Kim, T.-S.; Kim, B. J. Importance of Critical Molecular Weight of Semicrystalline n-Type Polymers for Mechanically Robust, Efficient Electroactive Thin Films. *Chem. Mater.* **2019**, *31*, 3163−3173.
(7) Root, S. E.; Savagatrup, S.; Printz, A. D.; Rodriquez, D.; Lipomi, D. J. Mechanical Properties of Organic Semiconductors for Stretchable, Highly Flexible, and Mechanically Robust Electronics. *Chem. Rev.* **2017**, *117*, 6467−6499.
(8) Wang, G.-J. N.; Gasperini, A.; Bao, Z. Stretchable Polymer Semiconductors for Plastic Electronics. *Adv. Electron. Mater.* **2018**, *4*, No. 1700429.
(9) Savagatrup, S.; Zhao, X.; Chan, E.; Mei, J.; Lipomi, D. J. Effect of Broken Conjugation on the Stretchability of Semiconducting Polymers. *Macromol. Rapid Commun.* **2016**, *37*, 1623−1628.
(10) Zheng, Y.; Ashizawa, M.; Zhang, S.; Kang, J.; Nikzad, S.; Yu, Z.; Ochiai, Y.; Wu, H.-C.; Tran, H.; Mun, J.; Zheng, Y.-Q.; Tok, J. B. H.; Gu, X.; Bao, Z. Tuning the Mechanical Properties of a Polymer Semiconductor by Modulating Hydrogen Bonding Interactions. *Chem. Mater.* **2020**, *32*, 5700−5714.
(11) Wu, H. C.; Lissel, F.; Wang, G. J. N.; Koshy, D. M.; Nikzad, S.; Yan, H.; Xu, J.; Luo, S.; Matsuhisa, N.; Cheng, Y.; Wang, F.; Ji, B.; Li, D.; Chen, W. C.; Xue, G.; Bao, Z. Metal−Ligand Based Mechanophores Enhance Both Mechanical Robustness and Electronic Performance of Polymer Semiconductors. *Adv. Funct. Mater.* **2021**, *31*, No. 2009201.
(12) Noriega, R.; Salleo, A.; Spakowitz, A. J. Chain conformations dictate multiscale charge transport phenomena in disordered semiconducting polymers. *Proc. Natl. Acad. Sci. U. S. A.* **2013**, *110*, 16315−16320.
(13) Gu, K.; Snyder, C. R.; Onorato, J.; Luscombe, C. K.; Bosse, A. W.; Loo, Y.-L. Assessing the Huang−Brown Description of Tie Chains for Charge Transport in Conjugated Polymers. *ACS Macro Lett.* **2018**, *7*, 1333−1338.
(14) Mollinger, S. A.; Salleo, A.; Spakowitz, A. J. Anomalous Charge Transport in Conjugated Polymers Reveals Underlying Mechanisms of Trapping and Percolation. *ACS Cent. Sci.* **2016**, *2*, 910−915.
(15) Jones, M. L.; Huang, D. M.; Chakrabarti, B.; Groves, C. Relating Molecular Morphology to Charge Mobility in Semicrystalline Conjugated Polymers. *J. Phys. Chem. C* **2016**, *120*, 4240−4250.
(16) Root, S. E.; Savagatrup, S.; Pais, C. J.; Arya, G.; Lipomi, D. J. Predicting the Mechanical Properties of Organic Semiconductors Using Coarse-Grained Molecular Dynamics Simulations. *Macromolecules* **2016**, *49*, 2886−2894.
(17) Yoshimoto, Y.; Sugiyama, S.; Shimada, S.; Kaneko, T.; Takagi, S.; Kinefuchi, I. Molecular Insights into the Mechanical Properties of Polymer−Fullerene Bulk Heterojunctions for Organic Photovoltaic Applications. *Macromolecules* **2021**, *54*, 958−969.
(18) Huang, D. M.; Faller, R.; Do, K.; Moule, A. J. Coarse-Grained Computer Simulations of Polymer/Fullerene Bulk Heterojunctions for Organic Photovoltaic Applications. *J. Chem. Theory Comput.* **2010**, *6*, 526−537.
(19) Lee, C.-K.; Pao, C.-W.; Chu, C.-W. Multiscale molecular simulations of the nanoscale morphologies of P3HT:PCBM blends for bulk heterojunction organic photovoltaic cells. *Energy Environ. Sci.* **2011**, *4*, 4124−4132.
(20) Schwarz, K. N.; Kee, T. W.; Huang, D. M. Coarse-grained simulations of the solution-phase self-assembly of poly(3-hexylthiophene) nanostructures. *Nanoscale* **2013**, *5*, 2017−2027.
(21) Lee, C.-K.; Pao, C.-W. Nanomorphology Evolution of P3HT/PCBM Blends during Solution-Processing from Coarse-Grained Molecular Simulations. *J. Phys. Chem. C* **2014**, *118*, 11224−11233.
(22) To, T. T.; Adams, S. Modelling of P3HT:PCBM interface using coarse-grained forcefield derived from accurate atomistic forcefield. *Phys. Chem. Chem. Phys.* **2014**, *16*, 4653−4663.
(23) Chen, C.-W.; Huang, C.-I. Effects of intra/inter-molecular potential parameters, length and grafting density of side-chains on the self-assembling behavior of poly(3′-alkylthiophene)s in the ordered state. *Polymer* **2015**, *77*, 189−198.
(24) Do, K.; Risko, C.; Anthony, J. E.; Amassian, A.; Brédas, J.-L. Dynamics, Miscibility, and Morphology in Polymer:Molecule Blends: The Impact of Chemical Functionality. *Chem. Mater.* **2015**, *27*, 7643−7651.
(25) Alessandri, R.; Uusitalo, J. J.; de Vries, A. H.; Havenith, R. W.; Marrink, S. J. Bulk Heterojunction Morphologies with Atomistic Resolution from Coarse-Grain Solvent Evaporation Simulations. *J. Am. Chem. Soc.* **2017**, *139*, 3697−3705.
(26) Martinez, L.; Andrade, R.; Birgin, E. G.; Martinez, J. M. PACKMOL: a package for building initial configurations for molecular dynamics simulations. *J. Comput. Chem.* **2009**, *30*, 2157−2164.
(27) Hoover, W. G. Canonical dynamics: Equilibrium phase-space distributions. *Phys. Rev. A* **1985**, *31*, 1695−1697.
(28) Ro, H. W.; Akgun, B.; O'Connor, B. T.; Hammond, M.; Kline, R. J.; Snyder, C. R.; Satija, S. K.; Ayzner, A. L.; Toney, M. F.; Soles, C. L.; DeLongchamp, D. M. Poly(3-hexylthiophene) and [6,6]-Phenyl-C61-butyric Acid Methyl Ester Mixing in Organic Solar Cells. *Macromolecules* **2012**, *45*, 6587−6599.
(29) Zhao, B.; Zikry, M. A. The effects of structural disorders and microstructural mechanisms on semi-crystalline P3HT behavior. *Polymer* **2015**, *57*, 1−11.
(30) Harris, K. D.; Elias, A. L.; Chung, H. J. Flexible electronics under strain: a review of mechanical characterization and durability enhancement strategies. *J. Mater. Sci.* **2015**, *51*, 2771−2805.
(31) Shi, X.; Liu, S.; Sun, Y.; Liang, J.; Chen, Y. Lowering Internal Friction of 0D-1D-2D Ternary Nanocomposite-Based Strain Sensor by Fullerene to Boost the Sensing Performance. *Adv. Funct. Mater.* **2018**, *28*, No. 1800850.
(32) Plimpton, S. Fast Parallel Algorithms for Short-Range Molecular Dynamics. *J. Comput. Phys.* **1995**, *117*, 1−19.
(33) Thompson, A. P.; Aktulga, H. M.; Berger, R.; Bolintineanu, D. S.; Brown, W. M.; Crozier, P. S.; in 't Veld, P. J.; Kohlmeyer, A.; Moore, S. G.; Nguyen, T. D.; Shan, R.; Stevens, M. J.; Tranchida, J.;

https://doi.org/10.1021/acs.macromol.3c01071
Macromolecules XXXX, XXX, XXX−XXX

Trott, C.; Plimpton, S. J. LAMMPS - a flexible simulation tool for particle-based materials modeling at the atomic, meso, and continuum scales. *Comput. Phys. Commun.* **2022**, *271*, No. 108171.
(34) Humphrey, W.; Dalke, A.; Schulten, K. VMD: Visual molecular dynamics. *J. Mol. Graphics* **1996**, *14*, 33−38.
(35) Mollinger, S. A.; Krajina, B. A.; Noriega, R.; Salleo, A.; Spakowitz, A. J. Percolation, Tie-Molecules, and the Microstructural Determinants of Charge Transport in Semicrystalline Conjugated Polymers. *ACS Macro Lett.* **2015**, *4*, 708−712.
(36) Rudnicki, P. E.; MacPherson, Q.; Balhorn, L.; Feng, B.; Qin, J.; Salleo, A.; Spakowitz, A. J. Impact of Liquid-Crystalline Chain Alignment on Charge Transport in Conducting Polymers. *Macromolecules* **2019**, *52*, 8932−8939.
(37) Vukmirovic, N.; Wang, L. W. Electronic structure of disordered conjugated polymers: polythiophenes. *J. Phys. Chem. B* **2009**, *113*, 409−415.
(38) Mozer, A. J.; Sariciftci, N. S. Negative electric field dependence of charge carrier drift mobility in conjugated, semiconducting polymers. *Chem. Phys. Lett.* **2004**, *389*, 438−442.
(39) Marcus, R. A.; Sutin, N. Electron-transfer reactions with unusual activation parameters. Treatment of reactions accompanied by large entropy decreases. *Inorg. Chem* **1975**, *14*, 213−216.
(40) Toman, P.; Mensik, M.; Bartkowiak, W.; Pfleger, J. Modelling of the charge carrier mobility in disordered linear polymer materials. *Phys. Chem. Chem. Phys.* **2017**, *19*, 7760−7771.
(41) Chen, X.; Guo, G.; Hao, Y.; Li, J.; Li, W.; Deng, J.; Zhang, G.; Zhai, M. First-principles investigation of band offset and charge transfer characteristics at the PE/fluorinated layer interface. *Phys. Chem. Chem. Phys.* **2020**, *22*, 22207−22216.
(42) O'Connor, B.; Kline, R. J.; Conrad, B. R.; Richter, L. J.; Gundlach, D.; Toney, M. F.; DeLongchamp, D. M. Anisotropic Structure and Charge Transport in Highly Strain-Aligned Regioregular Poly(3-hexylthiophene). *Adv. Funct. Mater.* **2011**, *21*, 3697−3705.
(43) Huang, Y.-W.; Lin, Y.-C.; Yen, H.-C.; Chen, C.-K.; Lee, W.-Y.; Chen, W.-C.; Chueh, C.-C. High Mobility Preservation of Near Amorphous Conjugated Polymers in the Stretched States Enabled by Biaxially-Extended Conjugated Side-Chain Design. *Chem. Mater.* **2020**, *32*, 7370−7382.
(44) Kröger, M. Shortest multiple disconnected path for the analysis of entanglements in two- and three-dimensional polymeric systems. *Comput. Phys. Commun.* **2005**, *168*, 209−232.
(45) Karayiannis, N. C.; Kröger, M. Combined Molecular Algorithms for the Generation, Equilibration and Topological Analysis of Entangled Polymers: Methodology and Performance. *Int. J. Mol. Sci.* **2009**, *10*, 5054−5089.
(46) Hoy, R. S.; Foteinopoulou, K.; Kröger, M. Topological analysis of polymeric melts: Chain-length effects and fast-converging estimators for entanglement length. *Phys. Rev. E* **2009**, *80*, No. 031803.
(47) Hoy, R. S.; Kröger, M. Unified Analytic Expressions for the Entanglement Length, Tube Diameter, and Plateau Modulus of Polymer Melts. *Phys. Rev. Lett.* **2020**, *124*, No. 147801.

https://doi.org/10.1021/acs.macromol.3c01071
Macromolecules XXXX, XXX, XXX−XXX